5ème Conférence Internationale des Energies Renouvelables (CIER– 2017)
Proceeding of Engineering and Technology –PET
Vol.28 pp.30-35

Optical study of quaternary chalcogenides materials: solar cell applications

ZIANE Mohamed Issam[1*], TABLAOUI Meftah[1], HAZI Imene[2], KHELFANE Amar[1]

[1]*Centre de Recherche en Technologie des Semi-conducteurs pour l'Energétique (CRTSE), 16000 Algeria*

[2]*Université SSAD DAHLEB de Blida, Faculté des sciences, département de Physique, 09000, Blida, Algeria.*

[*]issam1308@yahoo.fr

***Abstract*— Bring by the desire to find other materials with new or improved properties, computational physics for materials quickly emerged as a very promising tool used in this materials science. In this study we report first principles calculations of optical properties of four quaternary compounds based chalcogenide by using the full potential-linearized augmented plane wave (FP-LAPW) within the framework of the density functional theory (DFT) as implemented in the wien2k code. The Cu_2ZnSnS_4, $Cu_2ZnSnSe_4$ crystalize in the kesterite (I-4) and stannite (I-42m) structure, whereas the $Zn_2CuInTe_4$ and $Cd_2CuInTe_4$ are a member of quaternary I-II_2–III–VI_4 compounds with cubic zinc-blende structure (F-43m). These quaternary materials have tetrahedrally coordinated crystal structures, and their properties are much more diverse given the increased number of elements, so they may have wide applications in optoelectronic, photovoltaic, thermoelectrics, magnetic and magneto-optical applications. As results, a good agreement was found when we compared our calculations to previously reported data. Results were given for electronic band gap, dielectric function, optical conductivity, energy loss function, index of refraction and absorption coefficient.**

***Keywords*— DFT, quaternary chalcogenides, band gap, optical properties.**

I. INTRODUCTION

Due to the development of industry, transport and communications, growth in world electricity consumption has been observed in recent decades. However, most of the electrical energy is produced by the combustion of non-renewable resources (oil, gas, nuclear), whose exhaustion period is estimated to be some decade. Moreover, this type of production is very polluting in terms of climate.

The development of renewable and non-polluting energy sources is therefore timely. Renewable energy sources include wind, marine and ocean flows, geothermal energy, and solar PV. The latter is a very powerful source of energy, where photovoltaic electricity is obtained by the direct transformation of sunlight into electricity by means of the photovoltaic cell. This production of electricity by photovoltaic conversion occurs within semiconductor materials, that they have the properties to release their charge carriers (electron and hole) after absorption of photons from sunlight. That is why, research efforts are running for the development of solar cell from abundant and less toxic elements.

As chalcogenides are extremely important because of their applications in various technologies, the knowledge of their physical properties is necessary. In this article, various optical properties of Cu_2ZnSnS_4, $Cu_2ZnSnSe_4$, $Cd_2CuInTe_4$ and $Zn_2CuInTe_4$ are investigated using density functional theory DFT.

II. COMPUTATIONAL DETAILS

An easy way to comply with the conference paper formatting requirements is to use this document as a template and simply type your text into it.

In this paper, the Kohn–Sham equations are solved for calculating the electronic and optical properties of the tetragonal Cu_2ZnSnS_4, $Cu_2ZnSnSe_4$, and the cubic $Cd_2CuInTe_4$ and $Zn_2CuInTe_4$ quaternaries chalcogenides compounds. In order to solve Kohn–Sham equations, the full potential linearized augmented plane waves (FPLAPW) method with generalized gradient approximation [1] and the proposed by Engel and Vosko in the form of EV-GGA [2] along with modified Becke-Johnson (mBJ) potential [3] within the framework of DFT are used. To handle the exchange and correlation energies for electronic configuration, TB-mBJ is used as an exchange potential. Details of the FP-LAPW method, formulas and the WIEN2k software utilized in these calculations can be found in Ref. 4. The Muffin-Tin radius RMT values used are 2.2, 2.4, 2.2, 2.0, 2.5, 2.5 and 2.5 a. u. (atomic units) for Cu, Sn, Zn, S, In, Cd, and Te atoms respectively.

III. RESULTS AND DISCUSSIONS

III.1. OPTICAL PROPERTIES

CZTS and CZTSe are quaternary semiconductor materials of type I2-II-IV-VI4. These new materials are derived from a binary compound of a common formula AN B_8-N (N = 1,2,3) which crystallize in the cubic zinc-blende structure. The derivatives of this zinc-blende structure, they can be; ternaries, such as the family of materials I-III-VI_2, which crystallize in a fundamental structure of tetragonal type chalcopyrite (space group I-42d); and quaternaries such as the case of CZTS and CZTSe which manifest in two different types of kesterite and stannite structure of space group I-4 and I-42m, respectively. As we can see from figure 1, the difference between these two structures is only in the position of the two atoms of zinc and copper.

ISSN 2356-5608

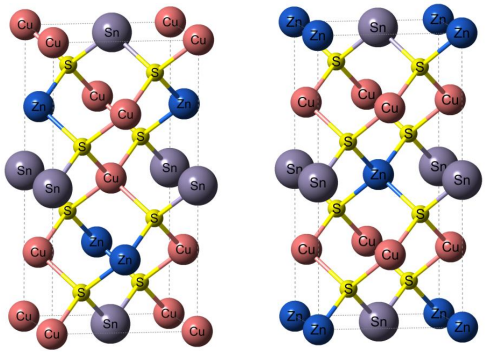

Fig. 1 Cristalline structure of kesterite (left) and stannite (right) of CZTS material.

Tellurides quaternary diamond-like structure represented by the general formulae A_2-I-III-VI_4 (A=Zn and Cd) are materials containing one or more chalcogenide elements (group VI in the periodic table, e.g. sulfur, selenium or tellurium) as a substantial constituent. Taking into account the chemical composition $A_2CuInTe_4$ (A=Zn and Cd), these quaternary materials have tetrahedrally coordinated crystal structures. $Zn_2CuInTe_4$ and $Cd_2CuInTe_4$ are a member of quaternary I-II_2–III–VI_4 compounds with cubic lattice. The structure of these compounds can be derived from the II–VI cubic structure. Nolas .etal. used powder x-ray diffraction and found that the polycrystalline $Zn_2CuInTe_4$ and $Cd_2CuInTe_4$ crystallize in cubic zinc blende structure [5]. The crystalline structures of our Tellurides compounds were simulated by using a supercell containing 16 non-equivalent atoms (2x2x2) in order to mimic the zinc blende structure with four different atoms. In figure 2 we presented as example the F-cubic structure of $Zn_2CuInTe_4$.

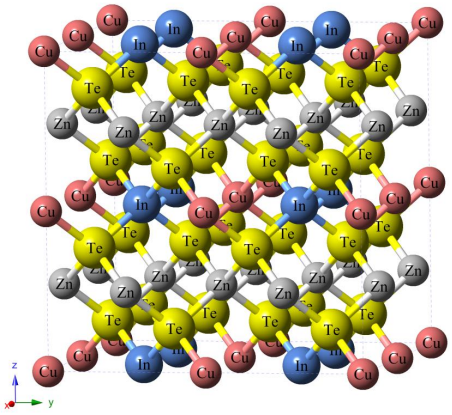

Fig. 2 Crystalline structure of $Zn_2CuInTe_4$.

The first step in calculating the first principle (ab-initio) is to find the optimized geometry of the crystal structure which plays a key role in investigating the properties of the ground state of materials. The lattice equilibrium parameters of a crystal are the lattices parameters that minimize the total energy of the system. In this study, we will present only the optical properties found with our optimized lattices parameters. The dielectric tensor is the key parameter for the determination of other optical parameters; it consists of nine independent components as a function of the symmetry of the crystal structure. In systems of isotropic character, as in the case of semiconductor that crystallize in a cubic structure, the dielectric tensor has only three identical diagonal components (εxx). Semiconductor compounds that crystallize in a structure other than the cubic lattice such as the tetragonal or hexagonal are uniaxial because they contain a special axis known as the optical axis (Oz).

As soon as the plane electromagnetic waves propagate in a specific direction along this optical axis, they have the same velocity at that instant independently of their direction of polarization. Along the other crystallographic axes, the material becomes anisotropic, where the velocity of light varies as a function of polarization.

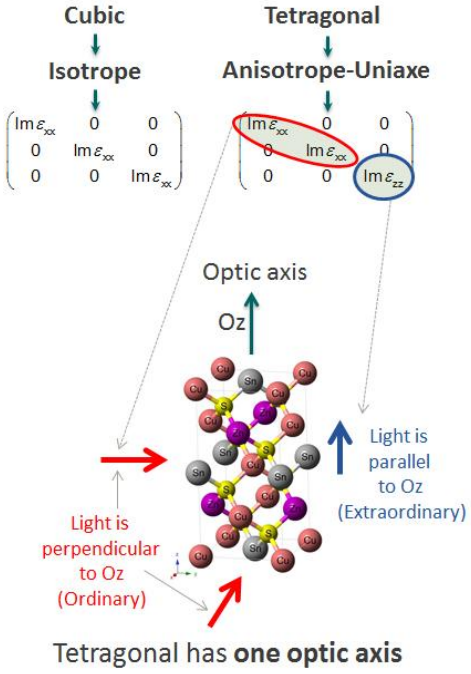

Fig. 3 Optical tensors in tetragonal structures.

The Kohn-Sham calculations provide matrix elements and joint densities of states necessary for the calculation of the complex dielectric function. The dielectric function is used to describe the system's linear spectral response to an electromagnetic radiation. The dielectric function is a complex function and is given by [6]

$$\varepsilon(\omega) = \varepsilon_1(\omega) + i\varepsilon_2(\omega) \qquad (1)$$

The real part $\varepsilon_1(\omega)$ can be derived from the imaginary part ε2(ω) of the dielectric function through the Kramers-Kronig relation [7]. The both quantities are given by the following well-known relations

$$\varepsilon_1(\omega) = 1 + \frac{2}{\pi} p\int_0^{\infty} \frac{\omega' \varepsilon_2(\omega')}{\omega'^2 - \omega^2} d\omega' \qquad (2)$$

$$\varepsilon_2(\omega) = \frac{e^2\hbar}{\pi m^2 \omega^2} \sum_{C,V} \int_{BZ} \left|M_{CV}(k)\right|^2 \delta\left[\omega_{CV}(k) - \omega\right] d^3k \qquad (3)$$

The values of the real and imaginary parts of the dielectric function dependent on photonic energy constitute a basis for deducing other optical quantities, such as the complex index of refraction with his real part (refractive index, n) and imaginary part (extinction coefficient, k) that are collectively called the optical constants of the solid.

$$n^*(\omega) = n(\omega) + ik(\omega) = \sqrt{\varepsilon(\omega)} = \sqrt{\varepsilon_1(\omega) + i\varepsilon_2(\omega)} \quad (4)$$

$$n(\omega) = \sqrt{\frac{(\varepsilon_1(\omega)^2 + \varepsilon_2(\omega)^2)^{1/2} + \varepsilon_1(\omega)}{2}} \quad (5)$$

$$\mathrm{Re}\,\sigma(\omega) = \frac{\omega}{4\pi}.\varepsilon_2 \quad (6)$$

$$\alpha(\omega) = \frac{2\omega}{c}.k \quad (7)$$

Where c is the speed of light in vacuum.

$$L(\omega) = \mathrm{Im}\left(-\frac{1}{\varepsilon(\omega)}\right) = \frac{\varepsilon_2}{\varepsilon_1(\omega)^2 + \varepsilon_2(\omega)^2} \quad (8)$$

The optical calculations discussed in this paper include full atomic relaxed structures. Using the wien2k code, it is feasible, though computationally demanding, to account fully for atomic relaxations by minimizing the forces. In other words, all the atoms in the quaternary alloy are allowed to relax from their nominal lattice positions until the strength of each of these atoms is reduced to a minimum. During relaxation, some correlations between the atomic positions defined in the inter-atomic distances served at reasonable values, and the adverse interactions are avoided.

TABLE I
CALCULATED BAND GAP COMPARED TO THE EXPERIMENTAL ONES

Materials	**Energy band gap**	
	Our TB-mBJ	**Experimental**
Cu_2ZnSnS_4-Ks		**1.5**[a]
no-relaxed	1.380	
relaxed	0.832	
Cu_2ZnSnS_4-St		**1.49**[b]
no-relaxed	1.209	
relaxed	0.741	
$Cu_2ZnSnSe_4$-Ks		**1.06**[c]
no-relaxed	0.990	
relaxed	0.525	
$Cu_2ZnSnSe_4$-St		**0.9**[d]
no-relaxed	0.78	
relaxed	0.327	
$Zn_2CuInTe_4$		**1.05**[e]
no-relaxed	1.260	
relaxed	0.848	
$Cd_2CuInTe_4$		**0.85**[e]
no-relaxed	0.931	
relaxed	0.840	

[a]Ref. [8] [b]Ref. [9] [c]Ref. [10] [d]Ref. [11] [e]Ref. [5]

In our calculations, a lorentzian broadening is taken at 0.1 for all our compounds. The scissors operator was also used in our calculation. The latter is added when the agreement between experimental and TB-mBJ obtained values of the band gap is often unsatisfactory (see table 1). In this study, the scissor operator values of 0.668, 0.749, 0.535, 0.573, 0.202 and 0.01 was used for CZTS-ks, CZTS-st, CZTSe-ks, CZTSe-st, ZnCITe and CdCITe, respectively.

The spectral variations of imaginary part of dielectric functions along xx axis are presented in figure 5. The obtained results were plotted for a radiation up to 16eV. The first critical point called threshold energy of $\varepsilon_2(\omega)$ curves are located at about 1 and 0.82eV, respectively for $Zn_2CuInTe_4$ and $Cd_2CuInTe_4$ compounds, and 1.44, 1.40, 0.96 and 0.78 for CZTS-Ks, CZTS-St, CZTSe-Ks and CZTSe-St, respectively. These critical points correspond to direct inter-band transitions from the highest valence band (formed by a mixture of Cu_d, Te_p and Cd_s states) and the lowest conduction band (In_s states) for $Zn_2CuInTe_4$ and $Cd_2CuInTe_4$ compounds. For CZTS-Ks, CZTS-St, CZTSe-Ks and CZTSe-St compounds, these critical points were from the maximum valence band formed by Cu_d states and the minimum conduction band of Sn_s. In the case of cubic compounds, the major peak move to higher energies and peak intensity increases with substitution of Cd by Zn element.

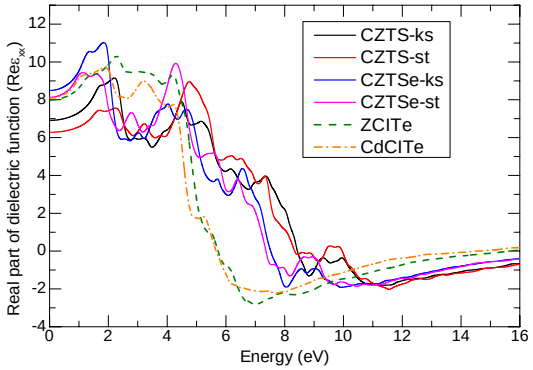

Fig. 4 Ordinary real part of dielectric function.

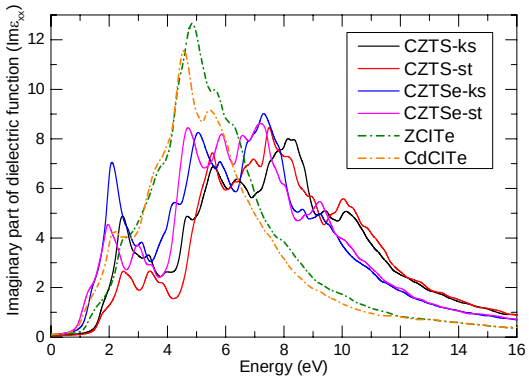

Fig. 5 Ordinary imaginary parts of dielectric function.

Since our study aims to predict and study the possibility of finding optoelectronic applications desirable to our materials, it is essential to study the anisotropy of the dielectric function and the birefringence in the complex refractive index.

The complex dielectric function represents the relationship between the electric and magnetic fields in a material. The real part tells us whether the material has a capacitive or inductive optical response. From Figures 4 and 6, we can clearly see that the evolution of the spectra of the complex

dielectric function is not identical along the two axis of directions x and z and the peaks are not located in the same photonic energies. The anisotropy in the stannite structures is more than in the kesterite ones for both CZTS and CZTSe materials. The peaks presented in these figures correspond to the inter-band electronic transitions between the valence and conduction bands. The important measurable quantity of the real part is its limit value at the zero frequency which is the electronic part of the static dielectric constant and which strongly depends on the value of the gap Eg. Calculated static dielectric constants are shown in Table II.

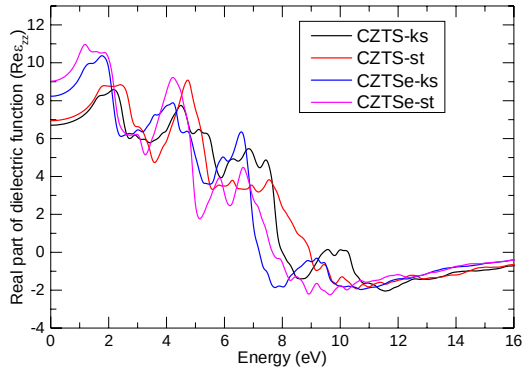

Fig. 6 Extraordinary real parts of dielectric function.

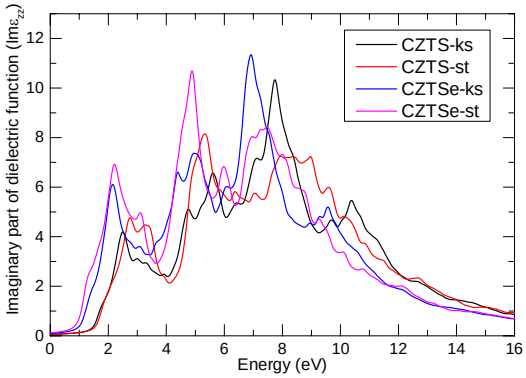

Fig. 7 Extraordinary imaginary parts of dielectric function.

TABLE II
CALCULATED TB-MBJ OPTICAL CONSTANTS

Materials	$\varepsilon_1(0)$	n_0	Δ_n	α_{max} .10^4	σ_{max} .10^4
Cu_2ZnSnS_4-Ks			-0.0396		
xx-direction	6.9115	2.6290		193.23	8.965
zz-direction	6.7049	2.5894		201.81	10.764
Cu_2ZnSnS_4-St			+0.1296		
xx-direction	6.2787	2.5057		201.22	8.539
zz-direction	6.9449	2.6353		193.17	8.728
$Cu_2ZnSnSe_4$-Ks			-0.0444		
xx-direction	8.4927	2.9142		177.86	8.886
zz-direction	8.2358	2.8698		183.25	10.569
$Cu_2ZnSnSe_4$-St			+0.1539		
xx-direction	8.1303	2.8514		179.35	8.395
zz-direction	9.0316	3.0053		179.65	8.482
$Zn_2CuInTe_4$			0		
xx-direction	7.9888	2.8265		153.24	8.299
$Cd_2CuInTe_4$			0		
xx-direction	8.0871	2.8438		141.29	7.138

When light is incident to such a surface, one part is reflected and the other crosses the middle. The refractive index is defined as the ratio between the speed light in the vacuum on its speed in the considered medium.

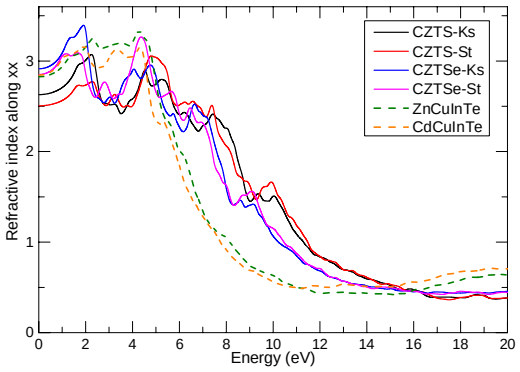

Fig. 8 Ordinary refractive indices.

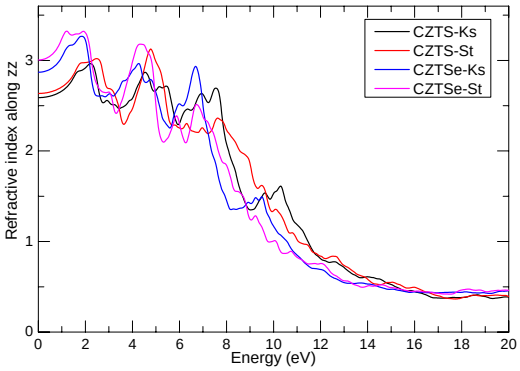

Fig. 9 Extraordinary refractive indices.

The imaginary part of the complex refractive index is the extinction coefficient or attenuation coefficient which measures the decay of the energy of the electromagnetic wave passing through the medium. The complex refractive indices calculated with the TB-mBJ approximation are presented in figures 8 and9 along xx and zz directions for photonic energies up to 16eV. For the kesterite structure, the refractive index reaches its maximum in the visible region, while for the stannite structure the latter is in the near ultraviolet range. The same remark was noted for the cubic structure. Also, the kesterite structures are negative birefringent materials, while the stannite structures have a positive birefringence. The values are noted in the table II. The case for cubic structures, the materials are isotropic and does not show a birifringence.

The reflectivity and the absorption coefficient are determined from the complex refection index. Reflectivity refers to the amount of reflected light incident on the surface. The absorption coefficient is qualified by the absorbency of the material.

In this sub-section, we are particularly interested in one phenomenon; the absorption, from which we can extract the absorption coefficient that it, can be calculated directly from the results obtained from the refractive index *n* and the extinction coefficient *k*, in the case of a normal incidence of the light on the surface of the sample.

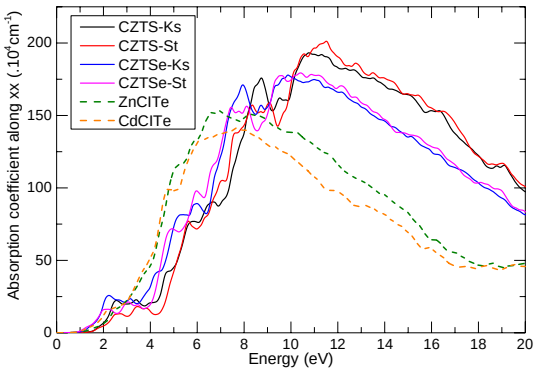

Fig. 10 Ordinary absorption coefficients.

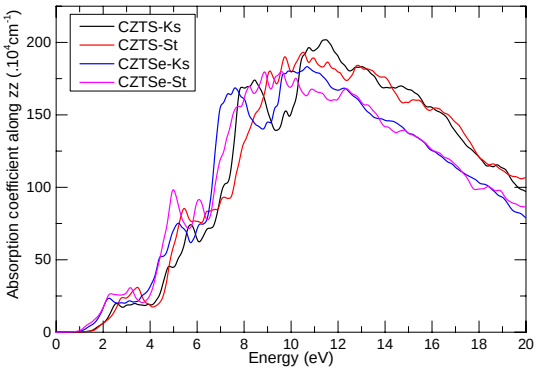

Fig. 11 Extraordinary absorption coefficients.

The spectral variations of the absorption coefficients for relaxed quaternaries calculated by the TB-mBJ approximation are plotted in figures 10 and 11. We calculated in these figures the absorption coefficient in the xx and zz direction along the optical axis Oz.

From these figures, an absorption coefficient equal to 0 for the photons possessing energy less than the energy band gap, it is in the IR region. A weak coefficient in the visible region and reaches its maximum in the UV region. The values the maximum absorption coefficient are noted in Table II. The stannite structure has a slightly higher absorption than the kesterite structure. When comparing our materials, we say that CZTS is the most absorbent material.

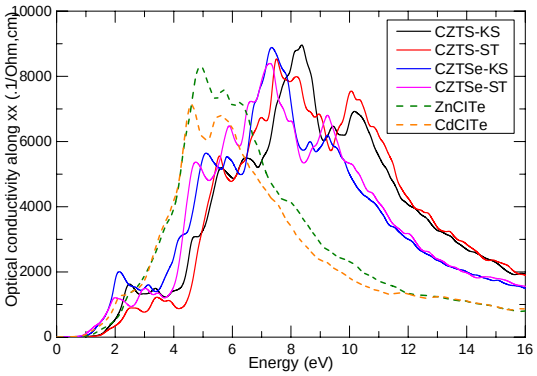

Fig. 12 Ordinary real parts of optical conductivity.

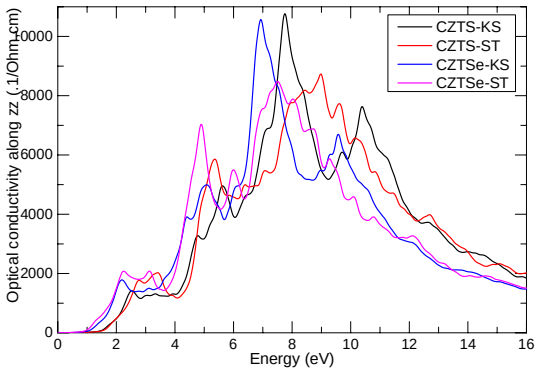

Fig. 13 Extraordinary real parts of optical conductivity.

The optical conductivity is an important means by which to study various aspects of a material. The optical conductivity gives information about the joint density of states of the bands between which the transition takes places. Physically, the linear response function of such material is a generalization of the electrical conductivity, which is usually considered in the static limit. The electronic optical conductivity of the compounds under study is plotted in figure 12 and 13, respectively along xx axis and zz. Closer inspection of figures 12 and 13 reveals that Zn2CuInTe4 and Cd2CuInTe4 cubic compounds have better optical conductivity properties in the region of 4 to 6eV than for the tetragonal materials such as CZTS and CZTSe. Also, the figure 13 clarifies that the optical conductivities in kesterite structures is more important than for the stannite ones along zz direction of light. Therefore, we can say that the kesterite structures are more favourable as absorbent layers compared to the stannite structure, in the case where the light is polarized parallel to the optical axis Oz.

The imaginary part of the reciprocal dielectric constant is called the energy loss function. The plasma response can be distinguished from an interband transition by the fact that both real and imaginary parts of the dielectric function are small in the vincity of the maximum in the loss function **[12]**. The electron energy loss function over the spectral region 0-40eV as calculated by TB-mBJ approximation for the equilibrium and relaxed structures. The frequency dependence of the imaginary part of the reciprocal dielectric constant peaks at the plasma frequency at about 22eV for CZTS, 20.9eV for CZTSe, 16eV for ZnCITe and 15.3eV for CdCITe compound. The plasma frequency for all our compounds corresponds to a wavelength in the ultraviolet spectral region of light.

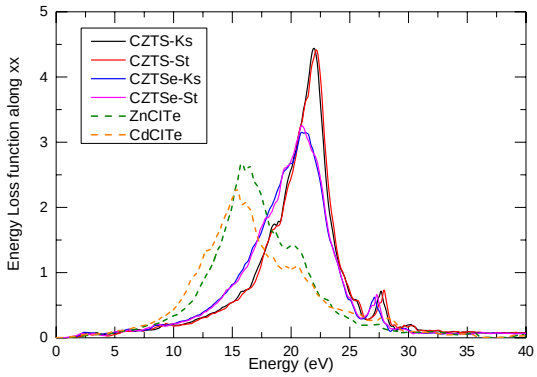

Fig. 14 Ordinary energy loss function.

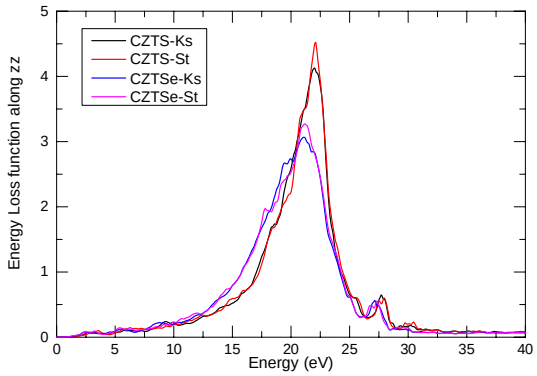

Fig. 15 Extraordinary energy loss function.

IV. Conclusions

Semiconductors are materials of great importance to electronic and optoelectronic devices because of the advantages that can be derived from the manipulation of their properties. Our work had the dual purpose of studying the fundamental properties of certain quaternaries chalcogenide materials and seeing the influence of the atom to be substituted on these properties. These questions were addressed using the WIEN2K computation code, combined with their theoretical approximations. As a conclusion, we can say that, the functional making uses of a good representation of the exchange-correlation term find in many cases a good estimation of the fundamental properties. The semiconducting materials CZTS, CZTSe, ZnCITe and CdCITe are optically active; hence, the optical properties of these materials in relaxed structures were investigated by using TB-mBJ approximation. In the tetragonal case, the calculation of the energy gaps proves that the kesterite structure has greater band gap energy than the stannite one. Our calculations indicate that the band gap in all our materials is direct. This quantity, we have shown, depends critically on the structural relaxation. From these calculations, we have clearly demonstrated that these compounds have a high absorption in the range of UV-Visible energy of the electromagnetic spectrum, and that these latter are not favorable to the use IR. According to this optical study, it might be interesting firstly to say not only that the two cubic materials are used in thermoelectric applications, but could also be considered as the good candidates for the design of possible optoelectronic devices operating in the visible and ultraviolet range.

References

[1] Z. Wu, R.E. Cohen, Phys. Rev. B. 73, 235116, 2006.
[2] E. Engel, S. H. Vosko, Phys. Rev. B47, 13164, 1993.
[3] F. Tran, P. Blaha, Phys. Rev. Lett. 102, 226401, 2009.
[4] P. Blaha, K. Schwarz, G. H. Madsen, D. Kvasnicka, J. Luitz, FP-LAPW+lo Program for Calculating Crystal Properties, K. Schwarz, Techn. WIEN2K, Austria 2001.
[5] George S. Nolas, M. Shafiq Hassan, Yongkwan Dong, Joshua Martin, Journal of Solid State Chemistry. 242 (2), 50-54, 2016.
[6] S. Adachi, *Properties of Semiconductor Alloys: Group-IV,III–V and II–VI Semiconductors*, Ed, John Wiley & Sons, Ltd., 2009.
[7] Anna Delin, Optics Communications 167, 105–109, 1999.
[8] P.M.P. Salomé, J. Malaquias, P.A. Fernandes, M.S. Ferreira, A.F. da Cunha, J.P. Leita~ o, J.C. Gonzalez, F.M. Matinaga, Solar Energy Materials & Solar Cells 101, 147–153, 2012.
[9] O. Mebktoub, T. Ouahrani et al, journal of alloys and compounds 653, 140-147, 2015.
[10] Kyoo-Ho Kim and Ikhlasul Amal, Electronic Materials Letters, Vol. 7, No. 3, pp. 225-230, 2011.
[11] G. Zoppi, I. Forbes, R. W. Miles, P. J. Dale, J. J. Scragg and L. M. Peter, Prog. Photovolt: Res. Appl.; 17, 315–319, 2009.
[12] Hari Singh Nalwa, Handbook of Advanced *Electronic and Photonic Materials and Devices*, 8nd ed., ACADEMIC PRESS, Ed. London, UK, 2001.